Sheet-current distribution in a dc SQUID washer probed by vortices

Dietmar Doenitz,[1] Matthias Ruoff,[1] Ernst Helmut Brandt,[2] John R. Clem,[3] Reinhold Kleiner,[1] and Dieter Koelle[1,*]

[1]*Physikalisches Institut-Experimentalphysik II, Universität Tübingen, Auf der Morgenstelle 14, 72076 Tübingen, Germany*

[2]*Max-Planck-Institut für Metallforschung, D-70506 Stuttgart, Germany*

[3]*Ames Laboratory, DOE and Department of Physics and Astronomy, Iowa State University, Ames, Iowa 50011, USA*

We present a method, based on vortex imaging by low-temperature scanning electron microscopy (LTSEM), to directly image the sheet-current distribution in $YBa_2Cu_3O_7$ dc superconducting quantum interference device washers. We show that the LTSEM vortex signals are simply related to the scalar stream function describing the vortex-free circulating sheet-current distribution $\mathbf{J}$. Unlike previous inversion methods that infer the current distribution from the measured magnetic field, our method uses pinned vortices as local detectors for $\mathbf{J}$. Our experimental results are in very good agreement with numerical calculations of $\mathbf{J}$.

PACS number(s): 74.78.−w, 68.37.Hk, 74.25.Op, 85.25.Dq

I. INTRODUCTION

Spatially resolved techniques can provide important insight into current flow, arrangement of vortices, flux pinning, and noise in superconductors and their mutual interactions. So far there has been only one method of imaging the current distribution in superconductors: The magnetic field distribution on top of a superconducting thin film is measured, e.g., by magneto-optics, from which the current distribution can then be calculated by inverting the Biot-Savart law.[1]

In this paper we present a method to directly image the sheet-current distribution in a $YBa_2Cu_3O_7$ thin film. We use low-temperature scanning electron microscopy[2–5] (LTSEM) to image vortices in dc superconducting quantum interference device (SQUID) washers.[6,7] Most techniques for vortex imaging, such as Lorentz microscopy,[8] scanning SQUID microscopy,[9,10] scanning Hall microscopy[11] or magneto-optics[12] rely on the detection of the stray magnetic field produced in close proximity to a vortex. In contrast, vortex imaging by LTSEM is different from those techniques, as it is based on the electron-beam-induced apparent displacement of a vortex, pinned at position $\mathbf{r}$ in the (x,y) plane of a SQUID washer, which is detected as a *change* of stray magnetic flux $\Phi(\mathbf{r})$ coupled to the SQUID. Hence, the contrast of the LTSEM vortex signals directly senses $\nabla\Phi(\mathbf{r})$. Recently, Clem and Brandt[13] have shown that $\Phi(\mathbf{r})$ is proportional to the scalar stream function $G(\mathbf{r})$ that describes the circulating sheet-current density $\mathbf{J}(\mathbf{r})$ flowing in the vortex-free case at position $\mathbf{r}$ in the SQUID washer. In this paper we show that this relationship allows us to use the vortices as local detectors for $\mathbf{J}(\mathbf{r})$: At each position a vortex has been imaged, we can directly determine $\mathbf{J}(\mathbf{r})$ without complicated calculations.

II. IMAGING OF PINNED VORTICES IN A SQUID WASHER

In our experiments, we investigated several dc SQUID washers [see Fig. 1(a)] fabricated from epitaxially grown d =80 nm thick c-axis-oriented $YBa_2Cu_3O_7$ (YBCO) thin films. We will present an analysis of LTSEM data obtained

from one representative device with washer size 120 μm × 305 μm, with a 100-μm-long and 4-μm-wide slit. The 1-μm-wide Josephson junctions are formed by a 24° symmetric grain boundary in the underlying $SrTiO_3$ substrate. For imaging by LTSEM, the YBCO SQUIDs are mounted on a magnetically shielded, liquid-nitrogen-cooled cryostage of an SEM (Ref. 14) and read out by a standard flux-locked loop (FLL) with 3.125-kHz bias-current reversal to eliminate $1/f$ noise due to fluctuations in the critical current I_c of the
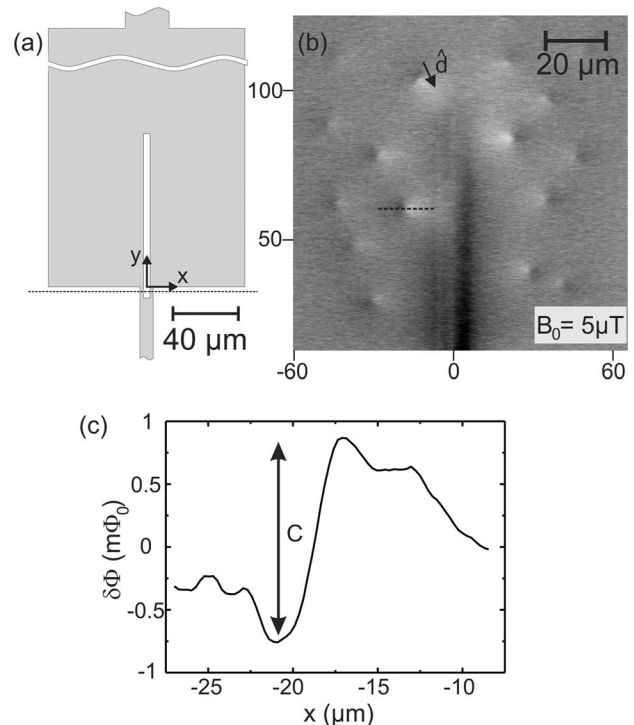

FIG. 1. (a) SQUID washer design; dotted line indicates grain boundary. (b) $\delta\Phi$ image of a washer SQUID. The arrow indicates the direction $\hat{\mathbf{d}}$ of one of the vortex signals. Tick labels are in units of μm. (c) Line scan $\delta\Phi(x)$ along the dashed line shown in (b). The signal contrast C—i.e., the difference between maximum positive and negative signals from a single vortex—is indicated by the arrow.

Josephson junctions. All LTSEM images are obtained at $T=77$ K after cooling the SQUID through T_c in a static magnetic field B_0.

For the spatially resolved measurements, the electron beam is used as a local perturbation that induces an increase in temperature $\delta T(x-x_0, y-y_0)$ on the sample surface (in the x, y plane) centered on the beam spot position (x_0, y_0). At $T=77$ K the length scale for the spatial decay of the thermal perturbation is set by the beam-electron range $R \approx 0.5$ μm for a typical beam voltage $V_b = 10$ kV.[4] This gives a maximum increase in beam-induced temperature ΔT of a few K at (x_0, y_0) for typical beam currents I_b of a few nA. So-called $\delta\Phi(x_0, y_0)$ images are obtained by recording the e-beam-induced flux change $\delta\Phi$ in the SQUID as a function of the e-beam coordinates (x_0, y_0). To improve the signal-to-noise ratio, we use a beam-blanking unit operating at typically 5 kHz, and the FLL output signal—i.e., the e-beam-induced flux change in the SQUID—is lock-in detected.

The mechanism of imaging of pinned vortices can be briefly described as follows: The e-beam-induced local increase in temperature produces a local increase in the Pearl length[15] $\Lambda = \lambda_L^2/d$, where λ_L is the temperature-dependent London penetration depth. Hence, the screening currents circulating around a pinned vortex are spatially extended due to e-beam irradiation. If the e beam is scanned across a vortex, the vortex's magnetic-field distribution is distorted in the direction of the beam spot; i.e., the center of the distorted field distribution is displaced by δr, which depends upon the distance of the beam spot from the vortex. This displacement changes the amount of stray magnetic flux $\Phi(\mathbf{r})$ in the negative z direction that a vortex at position $\mathbf{r}$ couples into the SQUID hole. Hence, scanning across a vortex induces a negative (positive) flux change $\delta\Phi$ in the SQUID if the vortex is moved away from (towards) the SQUID hole. Figure 1(b) shows an example of a $\delta\Phi$ image with vortices appearing as pairs of positive (bright) and negative (dark) signals.

III. RELATION BETWEEN THE LTSEM VORTEX SIGNAL AND SHEET CURRENT

Figure 1(c) shows a line scan $\delta\Phi(x)$ of the vortex signal along the dashed line shown in Fig. 1(b). The difference between the maximum positive and negative signals from a single vortex defines the contrast C of a vortex in the $\delta\Phi$ image. The contrast C depends on the maximum vortex displacement Δr, which is independent of the vortex position, and on the gradient of the function $\Phi(\mathbf{r})$. Neglecting the (small) variation in $|\nabla\Phi(\mathbf{r})|$ within Δr, we can write

$$C = 2\Delta r |\nabla\Phi(\mathbf{r})|. \qquad (1)$$

We define the direction $\hat{\mathbf{d}}$ of a vortex signal [cf. Fig. 1(b)] as the direction of a unit vector in the (x, y) plane pointing from the maximum negative to maximum positive signal of the vortex. Hence, $\hat{\mathbf{d}}$ is parallel to the gradient of $\Phi(\mathbf{r})$ and given as

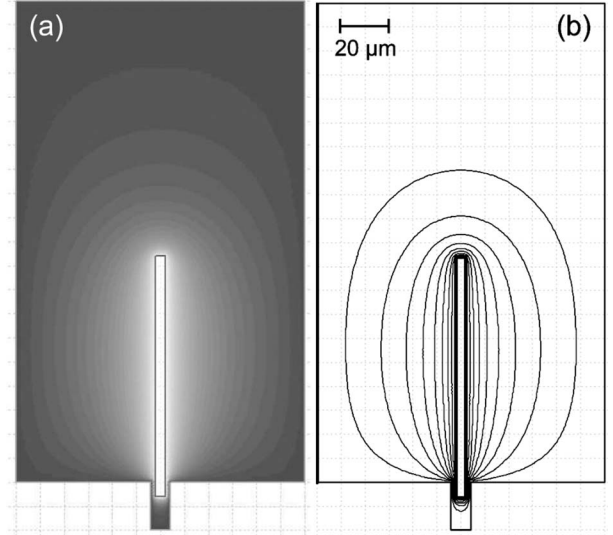$$\hat{\mathbf{d}} \equiv \nabla\Phi(\mathbf{r})/|\nabla\Phi(\mathbf{r})|. \qquad (2)$$

FIG. 2. Numerical simulation for a SQUID washer in the vortex-free case: (a) scalar stream function G; $G=1$ (white) at the slit edge; $G=0$ (black) at the outer edge and (b) streamlines, showing the current distribution in the SQUID washer.

In the vortex-free case and for currents below the critical current of the Josephson junctions, the SQUID washer acts as a closed superconducting loop, which can carry a persistent supercurrent I, flowing clockwise or counterclockwise. The sheet-current density $\mathbf{J}(\mathbf{r})$ is divergence free; thus, it can be written as

$$\mathbf{J}(\mathbf{r}) = I\hat{z} \times \nabla G(\mathbf{r}), \qquad (3)$$

where $\hat{z}$ is the unit vector in the direction perpendicular to the film plane and $G(\mathbf{r})$ is a stream function. $G(\mathbf{r})$ depends on the Pearl length, the film thickness, and the washer geometry; it can be chosen such that $G=0$ on the outer edge and $G=1$ on the inner edge of the SQUID.[13] This situation corresponds to the "trapped-flux case" (zero applied field, magnetic flux trapped in the hole and slit, which is bridged at the edge) shown in the upper left plot of Fig. 1 in Ref. 16.

While the function $\Phi(\mathbf{r})$ applies for the *vortex state* of the SQUID washer and the function $G(\mathbf{r})$ applies for the *vortex-free state*, Clem and Brandt used an energy argument to show that both functions are closely related[13] as

$$G(\mathbf{r}) = \frac{\Phi(\mathbf{r})}{\Phi_0}, \qquad (4)$$

where $\Phi_0 = h/2e$ is the magnetic flux quantum. This equation holds as long as the vortex cores do not overlap. This requirement is well fulfilled in our experiments since the applied fields are small (up to 40 μT) and thus the distance between the vortices is a few μm or more, well above $\Lambda \approx 0.5$ μm at $T=77$ K.
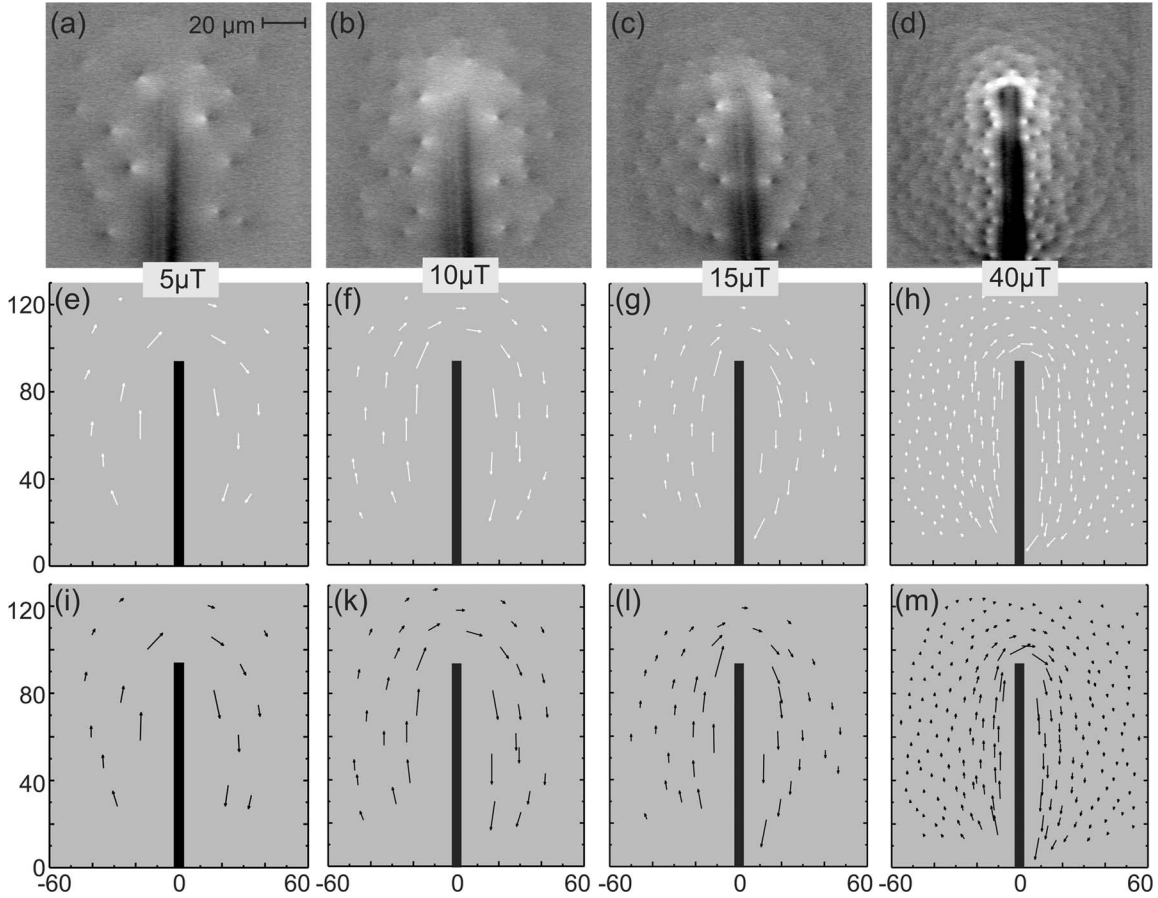
From Eqs. (1)–(4) one obtains

FIG. 3. Upper row: LTSEM $\delta\Phi$ images for different cooling fields B_0. Middle row: magnitude and direction of the sheet-current density calculated from the corresponding $\delta\Phi$ images (white arrows). Bottom row: magnitude and direction of sheet-current density calculated by numerical simulation of $\boldsymbol{J}(\boldsymbol{r})$ (black arrows). Tick labels are in units of μm.

$$J(r) = \frac{C}{\Phi_0}\frac{I}{2\Delta r}(\hat{z}\times\hat{d}); \qquad (5)$$

i.e., $|\boldsymbol{J}(\boldsymbol{r})|\propto C$ and $\boldsymbol{J}\perp\hat{\boldsymbol{d}}$. The magnitude of the vortex-free sheet-current density $\boldsymbol{J}$ at the position $\boldsymbol{r}$ of an imaged vortex is proportional to the contrast C of the LTSEM signal given by that vortex, while the direction of $\boldsymbol{J}$ is perpendicular to the direction $\hat{\boldsymbol{d}}$ of the vortex signal. These properties allow us to use the pinned vortices as local probes for the magnitude and direction of $\boldsymbol{J}$.

IV. COMPARISON OF EXPERIMENT WITH NUMERICAL SIMULATIONS

In order to check the validity of Eq. (5) we calculated the scalar stream function $G(\boldsymbol{r})$ and the vortex-free sheet-current density $\boldsymbol{J}(\boldsymbol{r})$ for the geometry of our SQUID washers, using the numerical simulation software package 3D-MLSI.[17] For the washer geometry in Fig. 1(a), $G(\boldsymbol{r})$ and $\boldsymbol{J}(\boldsymbol{r})$ are shown in Figs. 2(a) and 2(b), respectively.

In Fig. 3 we compare experimental data obtained from four $\delta\Phi$ images at different cooling fields (upper row) with the numerically calculated sheet-current distribution $\boldsymbol{J}(\boldsymbol{r})$. In

Figs. 3(e)–3(h) (middle row) every vortex imaged by LT-SEM is represented by a white arrow at the position of the imaged vortex. The direction of this arrow is perpendicular to $\hat{\boldsymbol{d}}$, and the length is proportional to the signal contrast C. From Eq. (5) it follows that the arrows should indicate the direction and magnitude of the normalized vortex-free sheet-current density $\boldsymbol{J}/I$. For comparison, Figs. 3(i)–3(m) (bottom row) show the results from numerical simulations; i.e., the black arrows represent the direction and magnitude of $\boldsymbol{J}(\boldsymbol{r})/I$. As shown in Fig. 3, the agreement between experimental data (middle row) and numerical simulation (bottom row) is very good. The rms deviations in magnitude and direction of the sheet-current density are given in Table I for four values of the cooling field. Since the proportionality constant between C and $\boldsymbol{J}/I$ contains Δr, which depends on experimental parameters such as e-beam power and sample temperature, we use Δr as a fitting parameter for each $\delta\Phi$ image (cf. Table I) to obtain the best agreement between experimental and numerical simulation data. There seems to be a trend towards smaller values of Δr with increasing B_0. The origin of this has not been clarified yet.

The deviations between experimental and simulation data for $\boldsymbol{J}/I$ can easily be explained by the difficulty in extracting the direction and magnitude of the vortex signals exactly. Furthermore, vortices imaged close to the Josephson junc-

TABLE I. rms deviation between experimentally determined and numerically calculated sheet-current density $J(r)$ and values for the maximum beam-induced displacement Δr.

Cooling field (μT)	rms deviation of magnitude	rms deviation of direction	Δr (nm)
5	16%	8.4°	52
10	20%	6.4°	43
15	19%	10.7°	41
40	26%	7.6°	40

tions yield a somewhat larger deviation in the direction of the sheet-current density as obtained from numerical simulations. During LTSEM imaging, shifts of the sample position up to a couple of μm in both the x and y directions may occur. While such a shift along the x direction can easily be corrected using the left and right (vertical) edges of the SQUID washer as a reference, a shift along the y direction cannot be corrected by using the bottom washer edge as a reference, since we avoided directly hitting the Josephson junctions with the e beam. In particular, for the largest cooling field $B_0 = 40$ μT, the analysis of the LTSEM data yields a significantly larger horizontal component for $|J|$ as compared to the numerically calculated current distribution [cf. Fig. 3(h) and 3(m)]. Most likely, this deviation is due to a vertical shift which occurs during LTSEM imaging. Except for the signals close to the Josephson junctions we did not find a systematic deviation between experimental and numerical data.

V. CONCLUSIONS

In conclusion, we have shown that the relation between the vortex-generated flux Φ in a SQUID washer and the scalar stream function G allows us to use the vortices as local detectors for the sheet-current distribution J in the vortex-free case. This is a more direct method of imaging circulat-

ing supercurrents that avoids complicated calculations. The experimental data obtained in magnetic fields up to 40 μT are in excellent agreement with numerical calculations of J, confirming both the validity of our model describing the generation of the LTSEM vortex signals and the validity of the relationship derived by Clem and Brandt,[13] even in the presence of many (up to 200) vortices in the SQUID washer.

Finally, we note that this technique for imaging the supercurrent distribution is by no means restricted to the very low magnetic fields applied in the present work. A standard SEM allows application of fields up to about 1 mT. For studies in larger fields, scanning laser microscopy can be used if the Josephson junctions can be properly shielded. Ultimately, the maximum applied field would be reached when the vortex spacing becomes smaller than the spatial resolution for vortex imaging. In our case, the latter is set by the beam electron range R, which depends on beam voltage and the substrate material. For beam voltages of a few kV, R is of the order of 100 nm. An Abrikosov lattice with 100 nm vortex spacing corresponds to a magnetic field of about 0.2 T. Furthermore, we note that our technique is not restricted to the simple rectangular washer geometry used in this work; it can be used for arbitrarily shaped geometries, as long as they can be integrated into a SQUID loop.

*Electronic address: koelle@uni-tuebingen.de

[1] C. Jooss, J. Albrecht, H. Kuhn, S. Leonhardt, and H. Kronmüller, Rep. Prog. Phys. **65**, 651 (2002).

[2] J. R. Clem and R. P. Huebener, J. Appl. Phys. **51**, 2764 (1980).

[3] R. P. Huebener, Rep. Prog. Phys. **47**, 175 (1984).

[4] R. Gross and D. Koelle, Rep. Prog. Phys. **57**, 651 (1994).

[5] T. Doderer, Int. J. Mod. Phys. B **11**, 1979 (1997).

[6] R. Straub, S. Keil, R. Kleiner, and D. Koelle, Appl. Phys. Lett. **78**, 3645 (2001).

[7] D. Doenitz, R. Straub, R. Kleiner, and D. Koelle, Appl. Phys. Lett. **85**, 5938 (2004).

[8] A. Tonomura *et al.*, Nature (London) **412**, 620 (2001).

[9] F. Tafuri, J. R. Kirtley, P. G. Medaglia, P. Orgiani, and G. Balestrino, Phys. Rev. Lett. **92**, 157006 (2004).

[10] J. R. Kirtley, C. C. Tsuei, M. Rupp, J. Z. Sun, L. S. Yu-Jahnes, A. Gupta, M. B. Ketchen, K. A. Moler, and M. Bhushan, Phys. Rev. Lett. **76**, 1336 (1996).

[11] A. N. Grigorenko, S. J. Bending, M. J. Van Bael, M. Lange, V. V. Moshchalkov, H. Fangohr, and P. A. J. de Groot, Phys. Rev. Lett. **90**, 237001 (2003).

[12] P. E. Goa, H. Hauglin, M. Baziljevich, E. Il'yashenko, P. L. Gammel, and T. H. Johansen, Supercond. Sci. Technol. **14**, 729 (2001).

[13] J. R. Clem and E. H. Brandt, Phys. Rev. B **72**, 174511 (2005). Our definitions of J, G, and Φ differ from those of J_d, G_d, and Φ_v in Ref. 13; they are related via $J = -J_d$, $G = 1 - G_d$, and $\Phi = \Phi_0 - \Phi_v$.

[14] R. Gerber, T. Nissel, H.-G. Wener, A. Willmann, R. Huebener, D. Koelle, and R. Gross, Cryogenics **37**, 21 (1997).

[15] J. Pearl, Appl. Phys. Lett. **5**, 65 (1964). The spatial dependence of the supercurrent and magnetic-field distributions is governed by the Pearl length when the film thickness d is less than λ_L, which is the case in the present experiments.

[16] E. H. Brandt, Phys. Rev. B **72**, 024529 (2005).

[17] M. Khapaev, M. Kupriyanov, E. Goldobin, and M. Siegel, Supercond. Sci. Technol. **16**, 24 (2003).